

THE TORQUING OF CIRCUMNUCLEAR ACCRETION DISKS BY STARS AND THE EVOLUTION OF MASSIVE BLACK HOLES

MICHAL BREGMAN AND TAL ALEXANDER

Dept. of Particle Physics and Astrophysics, Faculty of Physics, Weizmann Institute of Science, P.O. Box 26, Rehovot 76100, Israel

Draft version 4.0 November 15, 2018

Abstract

An accreting massive black hole (MBH) in a galactic nucleus is surrounded by a dense stellar cluster. We analyze and simulate numerically the evolution of a thin accretion disk due to its internal viscous torques, due to the frame-dragging torques of a spinning MBH (the Bardeen-Petterson effect) and due to the orbit-averaged gravitational torques by the stars (Resonant Relaxation). We show that the evolution of the MBH mass accretion rate, the MBH spin growth rate, and the covering fraction of the disk relative to the central ionizing continuum source, are all strongly coupled to the stochastic fluctuations of the stellar potential via the warps that the stellar torques excite in the disk. These lead to fluctuations by factors of up to a few in these quantities over a wide range of timescales, with most of the power on timescales $\gtrsim (M_\bullet/M_d)P(R_d)$, where M_\bullet and M_d are the masses of the MBH and disk, and P is the orbital period at the disk's mass-weighted mean radius R_d . The response of the disk is stronger the lighter it is and the more centrally concentrated the stellar cusp. As proof of concept, we simulate the evolution of the low-mass maser disk in NGC 4258, and show that its observed $O(10^\circ)$ warp can be driven by the stellar torques. We also show that the frame-dragging of a massive AGN disk couples the stochastic stellar torques to the MBH spin and can excite a jitter of a few degrees in its direction relative to that of the disk's outer regions.

Subject headings: galaxies: nuclei — galaxies: active — black hole physics — stars: kinematics and dynamics — accretion disks — galaxies: individual (NGC 4258)

1. INTRODUCTION

Massive black holes (MBH) gain most of their mass, and presumably a substantial fraction of their spin, in the course of luminous accretion (Soltan 1982; Yu & Tremaine 2002). This implies accretion via a radiatively efficient, geometrically thin and optically thick accretion disk. As the MBH mass grows, and in the absence of strong external perturbations (e.g. galactic mergers), the stellar population around it is expected to settle into a centrally concentrated cusp, $n_\star \propto r^{-\gamma}$ with $0.5 \lesssim \gamma \lesssim 2.5$, whether adiabatically (e.g. Young 1980), or by two-body relaxation (Bahcall & Wolf 1977; Alexander & Hopman 2009). This stellar cluster, which spatially coexists with the disk and extends farther out to a substantial fraction of the MBH's radius of dynamical influence (Merritt 2006, Fig. 12), can affect the disk both directly, via hydrodynamical interactions (e.g. Syer et al. 1991; Artymowicz et al. 1993; Vilkoviskij & Czerny 2002), and indirectly, by purely gravitational interactions (Bregman & Alexander 2009, hereafter BA09), and thereby possibly influence the cosmic evolution of MBHs. As we argue below (Section 1.3), unless the disk is very compact, it is the gravitational interactions that exert the dominant effect by deforming the disk's geometry.

The best known example of a deformed thin Keplerian accretion disk is that of the circumnuclear maser disk of active galaxy NGC 4258, which displays an $O(10^\circ)$ warp on the 0.1 pc scale. In a previous preliminary test of concept study (BA09), we analyzed the physical scales in the problem, and argued that the observed warp is consistent with resonant torquing of the disk by random fluctuations in the stellar distribution around the MBH. Here we extend and generalize that study by simulating numerically the evolution of a thin accretion disk due to its internal viscous torques, due to the frame-dragging torques of a spinning MBH and the

stellar orbit-averaged gravitational torques. We revisit the NGC 4258 maser disk, and further explore the implications of stellar torquing for an accretion disk's geometry, mass accretion rate and covering factor, and for the spin evolution of MBHs.

The paper is organized as follows. In the remainder of the introduction we describe a simplified model for a galactic nucleus harboring an accreting MBH, and scale it to the NGC 4258 system (Section 1.1). We then briefly review Resonant Relaxation (RR, Section 1.2) and derive some relevant order of magnitude estimates (Section 1.3). In Section 2 we describe how the MBH / disk / stellar cluster system is modeled and simulated numerically (a brief summary of the numerical scheme is presented in appendix A). We present the results in Section 3 and discuss and summarize them in Section 4.

1.1. The NGC 4258 system

Maser-emitting nuclear accretion disks are unique, clean probes of the environment near MBHs. The first discovered and best-studied maser disk, NGC 4258, is also the thinnest and most Keplerian (to better than 1%; Maloney 2002) nuclear disk yet discovered. Radio observations of H₂O maser emission from the edge-on disk (Greenhill et al. 1995) reveal the disk morphology, gas velocities and accelerations, and allow accurate measurements of the MBH mass ($M_\bullet = 3.7 \times 10^7 M_\odot$), the distance to the host galaxy ($D = 7.2 \pm 0.3$ Mpc) and the spatial extent of the maser region ($R_a = 0.13$ pc to $R_b = 0.26$ pc) (Herrnstein et al. 1996, 1999). Together with optical and X-ray observations, these also constrain the disk's accretion rate ($10^{-6} < \dot{M} < 10^{-4} M_\odot \text{ yr}^{-1}$) (Neufeld & Maloney 1995). The NGC 4258 maser disk shows a clear $O(10^\circ)$ warp (Herrnstein et al. 1996). It is noteworthy that observations also indicate possible warps in the maser disks of Circinus (Greenhill et al. 2003) and NGC 3393

(Kondratko et al. 2008).

Here the stellar cusp around the MBH is modeled as a single mass power-law cusp of stars, $N_*(< r) = N_h (r/r_h)^{3-\gamma}$, which extends inward from the radius of influence at $r_h = GM_\bullet/\sigma_b^2$, where the velocity dispersion of the galactic bulge σ_b can be estimated from the empirical M_\bullet/σ relation (Ferrarese & Merritt 2000; Gebhardt et al. 2003; Shields et al. 2003), and contains $N_h = \mu_h M_\bullet/M_\star$ stars of mass M_\star each, where $\mu_h \sim O(1)$. We model NGC 4258 with $r_h = 7$ pc, and assume $\mu_h = 2$ (the formal value for an MBH-less singular isothermal distribution, $M_\star = 1 M_\odot$, and unless stated otherwise, $\gamma = 1.75$ (a dynamically relaxed cusp, Bahcall & Wolf 1976). For the purpose of simulating the torques on the maser disk of NGC 4258, only stars in the radial range 0.01 pc to r_h are considered. The maser disk model is described in detail in Section 2.2.

1.2. Resonant relaxation

Resonant relaxation (Rauch & Tremaine 1996; Rauch & Ingalls 1998; Hopman & Alexander 2006) is a rapid angular momentum relaxation mechanism that operates in potentials with a high degree of approximate symmetry, which restricts orbital evolution (e.g. fixed ellipses in a nearly Keplerian potential, or fixed planar rosettes in a nearly spherical potential). In such potentials the fixed, orbit-averaged, stellar mass distribution exerts a constant residual torque on a test mass, which persists over a coherence time t_0 as long as perturbations due to deviations from the perfect symmetry remain small. The accumulated change in angular momentum \mathbf{J} over t_0 then becomes the “mean free path” in \mathbf{J} -space for the noncoherent random walk phase on timescales longer than t_0 . When t_0 is long, the mean free path is large and the random walk is rapid. The efficiency of RR is determined by the nature of the physical process that perturbs the symmetry and limits t_0 (e.g. the Keplerian symmetry is perturbed far from the MBH by the potential of the stars and near it by relativistic precession). For circular orbits in a near spherical potential, such as those of gas streams in an accretion disk, the RR torques can only change the orbital orientation, but not the eccentricity, i.e. $J(r) = J_c(r) = \text{const}$ (Gürkan & Hopman 2007), where $J_c = \sqrt{GM_\bullet r}$ is the maximal (circular) angular momentum at radius r . On timescales $t < t_0$, the direction of the angular momentum vector of a circular orbit of radius r changes coherently due to the residual forces by stars on the same scale,

$$w(r) \equiv |\Delta J_\perp(r)|/J_c(r) = \beta_\perp \sqrt{N_\star(r)} (M_\star/M_\bullet) t/P(r), \quad (1)$$

where N_\star is the number of stars within r and P is the orbital period. The numeric prefactor $\beta_\perp \sim O(1)$ may depend somewhat on the parameters of the cusp, and can be determined from N -body simulations, where it is measured to be $\beta_\perp \gtrsim \sqrt{2}$ (Eilon et al. 2009; Kupa & Alexander 2011, in prep.); $\beta_\perp = \sqrt{2}$ is adopted here. The “warp factor” w ($0 \leq w \leq 2$) corresponds to a tilt in \mathbf{J} by $\cos i = 1 - w^2/2$.

In the limit where the disk mass M_d is negligible compared to the MBH mass M_\bullet , the coherence time is set by the randomizing effect of RR itself on the torquing stars (“self-quenching”). In this case, the coherence time for the torque on a circular orbit of radius r by stars on the same scale is

$$t_{\text{sq}}(r) \sim A_{\text{sq}} (M_\bullet/M_\star) P(r) / \sqrt{N_\star(r)}, \quad (2)$$

where A_{sq} is an $O(1)$ numeric prefactor. Preliminary analysis

of N -body simulations indicates that $A_{\text{sq}} = 1.0 \pm 0.1$ (Kupa & Alexander 2011, in prep.); $A_{\text{sq}} = 1$ is adopted here. The warp factor grows over the self-quenching time to $w(t_{\text{sq}}) = \beta_\perp A_{\text{sq}} \approx \sqrt{2}$, that is, quenching occurs when the accumulated tilt in the orbital direction grows to $i \simeq \pi/2$. An approximate correction for the coherence time when the back reaction of the disk on the stars cannot be neglected, is introduced in Section 1.3.

1.3. Order of magnitude estimates

We argue here, based on an approximate analysis of scales, that purely gravitational interactions between the stars and the disk, rather than hydrodynamic ones, typically dominate the torquing of the disk; that around lower mass MBHs ($\lesssim 10^7 M_\odot$) the disk warps in response to the stellar torques, while around more massive MBHs it changes its orientation as a nearly rigid body; and that stellar torques are expected to warp the maser disk of NGC 4258 by $O(10^\circ)$.

Direct stars / disk interactions — Stars crossing the disk exert a torque on it by direct hydrodynamic interaction. To assess whether this effect competes with the purely gravitational RR torques, we estimate the torque exerted on the disk in reaction to the ram pressure the disk exerts on the stars. The residual torque by N_\star stars of mass M_\star and radius R_\star , on randomly oriented orbits, in a volume of size R enclosing a disk of mass M_d , is

$$T_{\text{ram}} \sim R F_{\text{ram}} \sim R \sqrt{N_\star} \rho v^2 \pi r_X^2, \quad (3)$$

where ρ is the disk density, $v^2 \sim GM_\bullet/R$, $r_X = \max(R_\star, r_B)$ is the effective cross-section radius of the star, where $r_B = 2GM_\star/(v^2 + c_s^2) \simeq 2(M_\star/M_\bullet)R$ is the Bondi radius in the limit $c_s \lesssim O(10 \text{ km s}^{-1}) \ll v \sim O(10^3 \text{ km s}^{-1})$, which holds for a cold accretion disk close to the MBH. For $M_\star = 1 M_\odot$, $R_\star = 1 R_\odot$, and for $M_\bullet = 3.7 \times 10^7 M_\odot$, $R = 0.26 \text{ pc}$ and $H/R = 0.002$ (the values for NGC 4258, Herrnstein et al. 2005), $r_X = R_\star$. The gas density can be estimated by $\rho \sim M_d/(\pi R^2 2H)$, where H is the disk’s exponential scale height. We further assume that the cold thin disk is close to its self-gravity stability limit (as implied by the non-smooth morphology of many observed galactic maser disks, Maloney 2002; Braatz & Gugliucci 2008, and is predicted to be the general case in AGN disks, Goodman 2003), $M_d/M_\bullet \sim H/R$. The ram torque is then

$$T_{\text{ram}} \sim R \sqrt{N_\star} \frac{M_d}{2\pi R^2 H} \frac{GM_\bullet}{R} \pi R_\star^2 = \frac{1}{2} \sqrt{N_\star} \frac{GM_\bullet}{R} \left(\frac{R_\star}{R} \right)^2, \quad (4)$$

while the residual RR torque on the disk by the stars is

$$T_{\text{RR}} \sim \sqrt{N_\star} \frac{GM_\star M_d}{R}. \quad (5)$$

The RR torques affect the disk continuously over an orbital time, whereas the ram torque is applied only twice per orbit, when the star crosses the disk. The ratio between the durations the torques are active is $\Delta t_{\text{ram}}/\Delta t_{\text{RR}} \sim 4H/(2\pi R)$, and therefore the ratio of accumulated changes in the disk angular momentum per orbital time is

$$\frac{\Delta J_{\text{ram}}}{\Delta J_{\text{RR}}} = \frac{T_{\text{ram}}}{T_{\text{RR}}} \frac{\Delta t_{\text{ram}}}{\Delta t_{\text{RR}}} = \frac{1}{\pi} \frac{M_\bullet}{M_\star} \left(\frac{R_\star}{R} \right)^2. \quad (6)$$

For the parameters of NGC 4258, $\Delta J_{\text{ram}}/\Delta J_{\text{RR}} \sim 10^{-7}$. Even if AGN disks are limited by gravitational instability to radii as

small as $R \sim 2000r_g$ ($r_g = GM_\bullet/c^2$), as argued by Goodman (2003), then $\Delta J_{\text{ram}}/\Delta J_{\text{RR}} \sim 0.02(M_\bullet/10^6 M_\odot)^{-1}$, and RR torquing dominates for all MBHs with mass $M_\bullet \gtrsim \text{few} \times 10^4 M_\odot$. The torquing of a thin disk by ram pressure is therefore negligible, and the torquing effects of the stars on the disk are well approximated by pure gravitational interactions.

Stellar torques vs. disk angular momentum transport— The effect of the RR torques on the disk geometry depends on the ratio between the stellar torques and the rate of angular momentum diffusion in the disk. When the internal viscous torques are small, differential torquing across the disk results in warps, which persist on the warp diffusion timescale $t_{\text{warp}} \sim (R/H)^2 P/2\pi\alpha_2$, where $\alpha_2 \sim O(1)$ is the dimensionless viscosity parameter associated with the vertical viscosity (Eq. 12). The necessary condition for the disk to be Keplerian, $N_\star \ll M_\bullet/M_\star$, and the condition for the warp to persist against diffusion, $t_0 < t_{\text{warp}}$, provide together a soft upper limit to the mass range of MBHs where disk warping is efficient,

$$M_\bullet < M_\star \left(\frac{R}{H}\right)^4 \frac{f_N}{4\pi^2\alpha_2^2}, \quad (7)$$

where $N_\star = f_N M_\bullet/M_\star$ is the number of stars out of the $N_h \sim O(M_\bullet/M_\star)$ in the MBH radius of influence that are close enough to the disk to affect it appreciably. Conversely, when $t_0 > t_{\text{warp}}$, the disk flattens out rapidly, and the stellar torquing results in an overall evolution in the inclination of the disk as a nearly rigid body. The upper limit for warping depends quite sensitively on the assumed parameters, especially the disk's aspect ratio. For $R/H = 250$, $f_N = 0.1$, $M_\star = 1 M_\odot$ and $\alpha_2 = 1$, it is $M_\bullet \sim O(10^7 M_\odot)$.

Residual stellar angular momentum— A random density perturbation on the spatial scale r has a Poisson magnitude $\sqrt{N_\star(r)}$ and carries angular momentum of the order $J_N \sim \sqrt{N_\star(r)} M_\star \sqrt{GM_\bullet r}$. This is the maximal angular momentum that can be transferred to the disk from that scale. The torque exerted by the stars on the disk will lead to an equal and opposite torque by the disk on the stars. By the time the disk has been torqued by J_N , the reaction force on the stars will disperse the perturbation, and another, uncorrelated one, will take its place. The back-reaction thus introduces a new coherence timescale for the perturbation, $t_{\text{react}}(r)$ such that $|\Delta \mathbf{J}(t_{\text{react}})| = J_N(r)$, which may be shorter than the self-quenching coherence timescale, t_{sq} and thus limit the action of the torques on the disk.

We estimate t_{react} here by approximating the disk, which extends between R_α and R_β , as a thin ring of mass M_d and mass-weighted mean radius $R_d = 2\pi M_d^{-1} \int_{R_\alpha}^{R_\beta} R^2 \Sigma dR$, and evaluating the stellar torque on the disk in the limits of small and large spatial scales. The lever arm on the gas disk is R_d . When $r \gg R_d$, the magnitude of the force by the stars on the disk is $\sqrt{N_\star(r)} GM_\star/r^2$, and so $\Delta J(t)/J_c(R_d) = \beta_\perp A_{\text{sq}}(R_d/r)^{1/2} t/t_{\text{sq}}(r)$. Conversely, when $r \ll R_d$, the force on the disk is $\sqrt{N_\star(r)} GM_\star/R_d^2$, and so $\Delta J(t)/J_c(R_d) = \beta_\perp A_{\text{sq}}(r/R_d)^{3/2} t/t_{\text{sq}}(r)$. In shorthand notation,

$$\Delta J(t)/J_c(R_d) = \beta_\perp A_{\text{sq}}(r/R_d)^{1/2-\Theta} t/t_{\text{sq}}(r), \quad (8)$$

where $\Theta = \text{sign}(r - R_d)$. The back-reaction timescale is then

$$t_{\text{react}}(r) = \frac{\sqrt{N_\star(r)} M_\star}{\beta_\perp A_{\text{sq}} M_d} \left(\frac{r}{R_d}\right)^\Theta t_{\text{sq}}(r) = \frac{1}{\beta_\perp} \frac{M_\bullet}{M_d} \left(\frac{r}{R_d}\right)^\Theta P(r), \quad (9)$$

which increases monotonically with r . The coherence time is $t_0(r, R_d) = \min(t_{\text{sq}}, t_{\text{react}})$. Since typically $t_{\text{react}}(r, R_d)/t_{\text{sq}}(r, R_d) = \sqrt{N_\star(r)}(M_\star/M_d)/\sqrt{2} < 1$ for $r \sim R_d$, where the stellar torques on the disk are most effective, the back-reaction time is what sets the limit on the coherence time. The change in the angular momentum of the disk over the back-reaction time is

$$w_{\text{react}}(r) = \sqrt{N_\star(r)} \frac{M_\star}{M_d} \sqrt{\frac{r}{R_d}}. \quad (10)$$

For the NGC 4258 cusp parameters (Section 1.1) and a disk mass of $M_d \sim 3000 M_\odot$ (Martin 2008; BA09) with $r \sim R_d \simeq 0.16$ pc, the predicted overall change in disk orientation is $\sim 27^\circ$, and the differential change across the inner and outer edges of the masing region, the observed warp angle ω , is an order unity fraction of that (BA09). We therefore anticipate that RR warping can lead to the $O(10^\circ)$ warp that is observed in NGC 4258.

2. CALCULATIONS

2.1. The evolution equation

The equation governing the evolution of the angular momentum surface density, \mathbf{L} , of a thin accretion disk under the influence of internal and external torques, is given in the limits of a Keplerian velocity field, no azimuthal modes and diffusive warp propagation ($\alpha_1 > H/R$), by (Papaloizou & Pringle 1983; Pringle 1992; Ogilvie 1999)

$$\begin{aligned} \frac{\partial \mathbf{L}}{\partial t} = & \frac{1}{R} \frac{\partial}{\partial R} \left[3R \frac{\partial}{\partial R} (v_1 L) \boldsymbol{\ell} + \frac{1}{2} v_2 R L \frac{\partial \boldsymbol{\ell}}{\partial R} \right] \\ & + \frac{1}{R} \frac{\partial}{\partial R} \left[\left(v_2 R^2 \left| \frac{\partial \boldsymbol{\ell}}{\partial R} \right|^2 - \frac{3}{2} v_1 \right) \mathbf{L} \right] \\ & + \frac{1}{R} \frac{\partial}{\partial R} \left[v_3 R \mathbf{L} \times \frac{\partial \boldsymbol{\ell}}{\partial R} \right] \\ & + \mathbf{T}_{\text{ext}} + \mathbf{T}_{\text{src}}, \end{aligned} \quad (11)$$

where $L = \Sigma \sqrt{GM_\bullet R}$, $\boldsymbol{\ell} = \mathbf{L}/L$ and Σ is the disk's mass surface density. The disk is thus effectively modeled as a set of concentric rigid thin annuli. The first term on the right-hand side of Eq. (11) describes the angular momentum that is carried to the central sink with the inflowing mass, the second term the angular momentum that is advected outward by the disk's internal viscous torques, which are expressed by the azimuthal kinematic viscosity v_1 (responsible for the mass inflow) and the vertical kinematic viscosity v_2 (responsible for the unwarping of the disk). The third term describes the precessional torque that accompanies large amplitude warps (Ogilvie 1999). We assume isotropic viscosities, $v_n = \tilde{\alpha}_n c_i H$ ($n = 1, 2, 3$), where c_i is the mid-plane isothermal sound speed, and use the second order expansion of the three dimensionless viscosity parameters

$$\tilde{\alpha}_n = A_n + B_n \psi^2 + O(\psi^4), \quad (n = 1, 2, 3) \quad (12)$$

in terms of the local dimensionless local warp amplitude $\psi = R |\partial \boldsymbol{\ell} / \partial R|$ (Ogilvie 1999; Lodato & Price 2010). The

first order coefficients are

$$A_1 = \alpha_1, A_2 = \frac{2(1+7\alpha_1^2)}{\alpha_1(4+\alpha_1^2)}, A_3 = \frac{3(1-2\alpha_1^2)}{2(4+\alpha_1^2)}. \quad (13)$$

We find that the 2nd order terms do not change the results significantly in our simulations. The second order coefficients are listed for completeness in appendix 2.3.1. For typical values $\alpha_1 < 1$, $v_2 \gg v_1$, that is, the disk unwraps faster than it flows into the MBH.

$\mathbf{T}_{\text{ext}} = \mathbf{T}_{\text{BP}} + \mathbf{T}_{\text{RR}}$ expresses the external torques per unit area applied to the disk, which here are those due to relativistic frame-dragging and to the stellar torques. \mathbf{T}_{src} expresses the torque per unit area due to a source term at the disk's outer edge (Section 2.3.1). The effect of frame dragging on the disk, the Bardeen-Petterson (BP) effect, is given to lowest post-Newtonian order by¹ (Bardeen & Petterson 1975)

$$\mathbf{T}_{\text{BP}} = \boldsymbol{\Omega}_{\text{LT}} \times \mathbf{L}, \quad (14)$$

where $\boldsymbol{\Omega}_{\text{LT}} = (2G/c^2 R^3) \mathbf{J}_\bullet$ is the Lense-Thirring precession angular frequency and $\mathbf{J}_\bullet = \chi GM_\bullet^2/c$ is the spin of the MBH, with $0 \leq |\chi| \leq 1$ the dimensionless spin parameter. The spin of the MBH evolves correspondingly by (King et al. 2005)

$$d\mathbf{J}_\bullet/dt = -2\pi \int_{R_\alpha}^{R_\beta} \mathbf{T}_{\text{BP}} R dR. \quad (15)$$

Since the torque is perpendicular to the MBH spin, it changes only its direction, not its magnitude. The BP torques work to align \mathbf{L} and \mathbf{J}_\bullet . The frame dragging torques dominate over the viscous torques out to the distance where the warp diffusion rate becomes faster than the Lense-Thirring precession rate, $R_{\text{BP}} = \sqrt{v_2(R_{\text{BP}})/\boldsymbol{\Omega}_{\text{LT}}(R_{\text{BP}})}$. Typically $R_{\text{BP}} \gg R_\alpha$. The integrand in Eq. (15) scales as $\Sigma(R)R^{-3/2}$, so the torque on the MBH is dominated by contributions from the innermost region of the disk that remains non-aligned, and can be estimated by $\dot{J}_{\text{BP}} \sim \pi R_{\text{BP}}^2 T_{\text{BP}}(R_{\text{BP}}) = \pi v_2(R_{\text{BP}}) \Sigma(R_{\text{BP}}) \sqrt{GM_\bullet R_{\text{BP}}}$. The timescale for the MBH spin to align itself with the disk is then $t_{\parallel} \sim J_\bullet/\dot{J}_{\text{BP}}$, which in steady-state ($\dot{M} \simeq 3\pi v_1 \Sigma$, $v_2 \simeq v_1/2\alpha_1^2$) can also be expressed as

$$t_{\parallel} = 6\chi\alpha_1^2 (M_\bullet/\dot{M}) \sqrt{r_g/R_{\text{BP}}}. \quad (16)$$

The torque on the MBH spin by direct accretion of matter, $\dot{J}_{\text{acc}} \sim \dot{M} \sqrt{GM_\bullet R_\alpha}$, can be neglected relative to that by the BP effect, \dot{J}_{BP} , since $\dot{J}_{\text{acc}}/\dot{J}_{\text{BP}} \sim 6\alpha_1^2 \sqrt{R_\alpha/R_{\text{BP}}} \ll 1$. Accretion can no longer be ignored on timescales long enough for it to change the MBH mass appreciably, $t \gtrsim t_E = \eta c \sigma_T / 4\pi G m_p = \eta 4.5 \times 10^8 \text{ yr}$, where t_E is the e -folding, or Salpeter, timescale for growth by Eddington-limited accretion, σ_T is the Thomson cross-section, m_p the proton mass and η the radiative efficiency of the accretion.

2.2. The internal structure of the disk

The internal structure of the disk needs to be specified to determine the viscosity. In the α -disk prescription, the mid-plane temperature T reflects the azimuthal kinetic viscosity of the disk via $v_1 = \alpha_1 c_i^2/\Omega_K$, where $c_i^2 = kT/\mu$ is the isothermal sound speed, μ is the mean molecular weight

¹ The divergence of the BP torque toward the center is softened by substituting $R \rightarrow \max(R, 300r_g)$.

and $\Omega_K = \sqrt{GM_\bullet/R^3}$ is the Keplerian angular frequency. The sound speed, in turn, determines the disk's exponential scale height $H = c_i/\Omega_K$.

The physical parameters of the masing region in the accretion disk of NGC 4258 can be inferred from the observed aspect ratio $H/R \sim 0.002$, which suggests a temperature of $T \sim 600 \text{ K}$ (Argon et al. 2007) for a gas pressure supported disk (observations disfavor magnetic support, see review by Lo 2005), and from the fact that H_2O maser emission is possible there. This requires the mid-plane molecular hydrogen density n_{H_2} to be in the range 10^7 cm^{-3} to 10^{11} cm^{-3} (all the hydrogen is assumed to be molecular), the mid-plane gas temperature T to be in the range $300 - 400 \text{ K}$ to 1000 K , and the mid-plane pressure p/k to be in the range $10^{10} \text{ K cm}^{-3}$ to $10^{13} \text{ K cm}^{-3}$ (Maloney 2002). In addition, stability against fragmentation requires that Toomre's criterion holds locally², $Q = c_i \Omega_K / \pi G \Sigma > 1$ (Toomre 1964), which further constrains the disk mass and temperature.

It is unclear whether the accretion disk's internal viscosity alone can provide enough heat to warm the molecular gas to masing temperatures. Neufeld & Maloney (1995) argue that heating by X-ray irradiation by the central source is essential for creating the required conditions in the masing region. Outside the masing region, the disk's properties are not usefully constrained by current observations.

Here we make a choice of convenience to adopt the known solution³ of a gas pressure-dominated thin accretion disk, where the temperature is completely determined by the internal viscosity (that is, no external heating) and free-free (Kramer's law) opacity (Shakura & Sunyaev 1973). The prefactor κ_a of Kramer's law, $\kappa = \kappa_a(\rho/\rho_a)(T/T_a)^{-7/2}$, where $\rho = \Sigma/(\sqrt{2\pi}H)$ is the total mid-plane mass density (the subscript a denotes values at R_a) is then adjusted to be high enough to maintain the required temperature at the masing region⁴. We assume Solar abundances ($X = 0.7057$, Arnett 1996) and that all the hydrogen is molecular, which corresponds to a mean molecular weight of $\mu = 2.358 m_p$. The adopted value $[H/R]_a = 0.002$ fixes the surface density $\Sigma_a = \rho_a \sqrt{2\pi} [H/R]_a R_a$, where $\rho_a = n_{\text{H}_2}(R_a) 2m_p/X$. We find that in order to have masing conditions between R_a and R_b , it is necessary to assume the highest temperature value at the inner edge, $T_a = 10^3 \text{ K}$. The assumed density there, $n_{\text{H}_2}(R_a) = 3 \times 10^8 \text{ cm}^{-3}$, which is within the masing range and consistent with the limits on $p_a/k = (\rho_a/\mu)T_a$, is chosen so the total disk mass is $3 \times 10^3 M_\odot$. The mid-plane temperature is given by $\sigma_{\text{SB}} T^4 = (27/32) \Sigma^2 \Omega_K^2 v_1 \kappa$ (e.g. Frank et al. 2002, Eq. 5.76), which here yields

$$T(R, t) = \left[\frac{27k_B^{1/2}}{\sqrt{2\pi} 32 \sigma_{\text{SB}}} \frac{\alpha_1 \kappa_a T_a^{7/2}}{\mu^{1/2} \rho_a} \Sigma^3(R, t) \Omega_K^2(R) \right]^{1/7}. \quad (17)$$

For the values of T_a and ρ_a above, Eq. (17) requires for self-consistency $\kappa_a = 7.195 \times 10^5 / \alpha_1 \text{ cm}^2 \text{ g}^{-1}$. This is an

² Toomre's criterion can be recast as an approximate global condition, $M(< R)/M_\bullet < c_i/v_K = H/R$, where $v_K = \sqrt{GM_\bullet/R}$.

³ The steady state solution has $T \propto R^{-3/4}$, $\Sigma \propto R^{-3/4}$, $c_i \propto R^{-3/8}$, $H \propto R^{9/8}$, $n_{\text{H}_2} \propto R^{-15/8}$, $v_1 \propto v_2 \propto R^{3/4}$, $p/k \propto R^{-21/8}$ and Toomre's $Q \propto R^{-9/8}$.

⁴ The actual opacity law in a cool molecular disk presumably resembles that of a proto-planetary disk, e.g. Semenov et al. (2003), which does not have a simple analytic form.

extremely high near/mid IR opacity ($\lambda_{\max} \sim 3 - 10 \mu\text{m}$ for $T \sim 300 - 1000 \text{K}$), as compared, for example, to the mean theoretical opacity of $\langle \kappa(2.2 \mu\text{m}) \rangle = 3800 \pm 700 \text{cm}^2 \text{g}^{-1}$ used to model dusty star forming cores (Shirley et al. 2011). This is in line with the conclusion that an external source of heating is required to explain the gas temperature.

2.3. Numerical implementation

The finite difference method is used to integrate the evolution equations (Eq. 11 with $G = c = M_\bullet = 1$) for the angular momentum surface densities $\{\mathbf{L}_i^j\}_{i=0}^{N+1}$ at time t_j , at positions $\{R_i\}_{i=0}^{N+1}$ on a logarithmically spaced grid between $R_1 = R_\alpha$ at the innermost stable circular orbit (ISCO) and $R_N = R_\beta \gg R_1$. The edge points R_0 and R_{N+1} are used to enforce the boundary conditions. A brief description of the numerical scheme (Papaloizou & Pringle 1983; Pringle 1992) is given in appendix A.

2.3.1. Initial conditions and boundary conditions

The initial conditions are a flat disk with surface density $\Sigma = \Sigma_a (R/R_a)^{-3/4}$ and normal ℓ_0 , where Σ is chosen so as to satisfy the maser conditions between the masing region limits R_a and R_b . The MBH spin is initially along the z -axis. We assume the boundary conditions $L(R_1) = 0$ and $\partial \ell / \partial R|_{R_1} = 0$ (central mass sink and no warp), and $\partial(v_1 \mathbf{L}) / \partial R|_{R_2} = 0$ (no torque). These boundary conditions allow mass through the inner boundary into the MBH. To prevent the disk from draining on the viscous timescale, and from drifting away from the masing conditions much before that, a source term is added at the outer edge. It is adjusted every time-step t_j to compensate for the mass lost from the disk, $(\Delta M)^j = \sum_{i=1}^N (M_i^j - M_i^{j-1})$, where $M_i^j = 2\pi R_i \Delta R_i \Sigma_i^j$ is the mass in a disk ring of width $\Delta R_i = R_i - R_{i-1} \ll R_i$. The angular momentum density at the outermost grid point is then augmented by an amount $(\Delta L_N)^j \ell_0$, such that $|\mathbf{L}_N^j + (\Delta L_N)^j \ell_0| = [\Sigma_N^j + (\Delta \Sigma_N)^j] \sqrt{R_N}$, where $(\Delta \Sigma_N)^j = -X_M (\Delta M)^j / 2\pi R_N \Delta R_N$ (X_M is an order unity stabilization factor, see below). The magnitude of the angular momentum needed to compensate for the mass loss is therefore

$$(\Delta L_N)^j = -\mathbf{L}_N^j \cdot \ell_0 + \sqrt{(\mathbf{L}_N^j \cdot \ell_0)^2 + [\Sigma_N^j + (\Delta \Sigma_N)^j]^2 R_N} - (L_N^j)^2. \quad (18)$$

The fluctuating factor $X_M = 1 \pm \varepsilon$ stabilizes the disk against the accumulation of numeric integration errors by allowing small over- or under-corrections, as needed⁵. When $(\Delta M)^j < 0$, X_M is set to $1 + \varepsilon$, and conversely, when $(\Delta M)^j > 0$, it is set to $1 - \varepsilon$. Experimentation indicates that $\varepsilon = 0.1$ is a good choice.

We find that with the source term thus defined, a flat disk with the inner boundary conditions $v_1 \Sigma|_{R_1} = 0$, rapidly converges to a close approximation of its theoretically expected steady state solution with the expected mass-loss rate of $\dot{M} \simeq 3\pi v_1 \Sigma$ (for $R \gg R_\alpha$). Likewise, the mass of a non-stationary disk rapidly converges to a steady state value that is typically within $O(10^{-3})$ of its initial mass, even as its geometry continuously changes. The mean accretion rate

⁵ This algorithm of stabilization by over-shooting is inspired by the engineering method of control system hysteresis, used e.g. in thermostats.

over some period t_{j_1} to t_{j_2} can then be estimated by $\langle \dot{M} \rangle = (\sum_{j=j_1}^{j_2} X_M (\Delta M)^j) / (t_{j_2} - t_{j_1})$.

This mass replenishment scheme represents an idealized case of a self-regulating mass supply, which prevents both the draining and over-loading and fragmentation of the disk. It should be emphasized that this assumption is introduced here for convenience only, to stabilize the disk long enough to collect robust statistics. Our statistical conclusions about the dynamical response of the disk to the external stellar torques do not depend strongly on the existence of such a mass source, as long as the disk mass is in quasi-equilibrium for at least the relatively short RR timescale.

2.3.2. The stellar resonant relaxation torques

The RR torques due to the $O(10^8)$ stars in the radius of influence cannot be modeled directly. Instead, they are approximated here by representing the stellar cusp by a small number of concentric spherical shells delimited by the radii $\{r_k\}_{k=0}^{N_s}$ (where $r_0 = 0$). The spacing between consecutive shell radii is chosen to be large enough so that the residual forces are approximately independent of each other, $r_{k+1}/r_k \geq 2^{2/(3-\gamma)}$, which corresponds to the requirement that $\sqrt{N_*(\langle r_k \rangle)} \geq 2\sqrt{N_*(\langle r_{k-1} \rangle)}$ (BA09), and is broadly consistent with the rigorous derivation of Kocsis & Tremaine (2011). The maximal number of such logarithmically spaced independent star shells in the simulations of NGC 4258 that are presented below is typically $N_s = 5$. The vector RR torques from each shell are represented by the gravitational field of a thin ring of mass $M_k = \sqrt{N_*(\langle r_k \rangle) - N_*(\langle r_{k-1} \rangle)} M_*$ with radius $\bar{r}_k = (r_k + r_{k-1})/2$ and normal $\mathbf{n}_k(t)$, which is interpolated smoothly in time by cubic spline from a sequence of isotropic random normals $\{\mathbf{n}_k^j\}_{j=0}^{\lfloor t_{\text{sim}}/t_0 \rfloor + 1}$ at times $t_j = jt_0(r_k)$, where t_{sim} is the duration of the simulation and $t_0(r) = \min(t_{\text{sq}}(r), t_{\text{react}}(r))$ (Eqs. 2, 9) is the coherence time. This simulates the random reorientation of the local residual force after a vector RR timescale. Finally, the torque exerted by a star ring at \bar{r}_k on a disk gas ring at R_i , which is directed along the line of intersection of the two rings, is calculated numerically by integrating over the gravitational force between all mass elements in the rings (Nayakshin 2005),

$$\mathbf{T}_{\text{RR}}(k \rightarrow i) = \frac{M_i M_k R_i \bar{r}_k}{(R_i^2 + \bar{r}_k^2)^{3/2}} \frac{\sin \beta}{4\pi^2} \times \quad (19)$$

$$\int_0^{2\pi} d\phi_1 \int_0^{2\pi} d\phi_2 \frac{\sin \phi_1 \sin \phi_2}{[1 - \delta \cos \lambda]^{3/2}} (\ell_i \times \mathbf{n}_k), \quad (20)$$

where M_i is the mass of the disk annulus, $\beta = \cos^{-1}(\ell_i \cdot \mathbf{n}_k)$, $\delta = 1 - (\bar{r}_k^2 - R_i^2) / (\bar{r}_k^2 + R_i^2)$ and⁶ $\cos \lambda = \cos \beta \sin \phi_1 \sin \phi_2 + \cos \phi_1 \cos \phi_2$.

2.3.3. Validation of the code

We verified that the numeric integration scheme conserves angular momentum to floating point precision, and conserves mass to a fractional precision of $O(10^{-10} \text{yr}^{-1})$, by switching off the source term and evolving a flat disk from an out-of-steady-state initial surface mass density profile ($\Sigma \propto R^{-1}$). We also evolved an $\Sigma \propto R^{-3/4}$ initial configuration with a

⁶ The divergence of the torque when $\bar{r}_k \rightarrow R_i$ is smoothed by substituting $\delta \rightarrow \delta - \max[(\bar{r}_k^2 - R_i^2), (\bar{r}_k - \bar{r}_{k-1})^2, (R_i - R_{i-1})^2] / (\bar{r}_k^2 + R_i^2)$.

source term at R_2 and with boundary conditions $v_1\Sigma = 0$ at R_1 , and verified it approximates the analytical solution $3\pi v_1\Sigma = \dot{M}(1 - \sqrt{R_1/R})$ (e.g. Frank et al. 2002) reasonably well (the match with the analytic solution is better on a linear grid than on a logarithmic one; overall the match on a logarithmic grid is at a level similar to that obtained by Pringle 1992). We also reproduce qualitatively the response of the disk to initial twists and to the BP torques that are presented by Pringle (1992).

3. RESULTS

We carried out a suite of disk evolution simulations, using a stellar cusp model based on NGC 4258 (Section 1.1) on a logarithmic grid with $N = 100$ points extending from $R_1 = 6r_g$ to $R_N = 1.5 \times 10^5 r_g$ ($r_g \simeq 5.5 \times 10^{12}$ cm $\simeq 1.8 \times 10^{-6}$ pc). The typical time-step increments in our simulations were in the range $\Delta t_j \sim 0.01$ –1 yr. The initial disk configuration was flat with a $\Sigma \propto R^{-3/4}$ surface mass density profile, and the disk was tilted by an angle i_0 relative to the z -axis, which coincided with the initial MBH spin, in those simulations with $\chi \neq 0$. In the simulations presented below, we explore the initial conditions $i_0 = 0, 3/4$ rad and $\chi = 0, 1$. At later times, we generalize the definition of the tilt angle to $i = \cos^{-1}(\mathbf{J}_\bullet \cdot \mathbf{J}_{\text{disk}}/J_\bullet J_{\text{disk}})$, where \mathbf{J}_{disk} is the total angular momentum of the disk. To isolate the effect of the BP torques on the disk, we ran some simulations with $N_\star = 0$. In the presence of RR, the disk never reaches a steady state, and the simulations are terminated after they are observed to reach statistical stationarity (recall that the mass supply rate is adjusted continuously to maintain constant total mass, Section 2.3.1). Simulations without RR are stopped when the relative rate of change in $\{\mathbf{L}_i\}_{i=1}^N$ falls below some very small value.

Figure (1) shows snapshots from a simulation of a misaligned disk ($i_0 = 3/4$ rad) evolving under both BP and RR torques, and the evolution of the inclination angle i for this and two other simulations, one with no RR and the other starting with an aligned disk ($i_0 = 0$ rad). The evolution from the initial (and artificial) misaligned configuration, where the disk is tilted relative to the MBH spin all the way down to R_1 , shows strong stochastic RR-dominated evolution that is superposed on a slower frame dragging-dominated secular evolution, until at later times the stochastic behavior dominates.

3.1. Disk warping

Figure (2) shows that RR-induced warping can easily reproduce the observed 8° warp angle across the maser region of NGC 4258 (Herrnstein et al. 2005), without requiring any particular initial conditions. The three scenarios explored here, RR with maximal ($\chi = 1$) frame-dragging and a large ($i_0 = 3/4$ rad) initial tilt, or with a small ($i_0 = 0$ rad) initial tilt, or without frame-dragging ($\chi = 0$), all exhibit a probability $P_8 \sim \mathcal{O}(1)$ to have $\omega \geq 8^\circ$ (see probabilities quoted in Figure 2). This should be contrasted with the scenario where only frame dragging is operating (Caproni et al. 2007). In the example shown here, the warp angle never exceeds 5° . By careful choice of the initial parameters, it may be possible to obtain a large enough warp angle, and satisfy the constraints set by the direction of the radio jet with frame dragging only. However, this requires considerable fine-tuning, and may require a very long-lived disk for the warp to grow (Martin 2008).

The warping probability increases with the steepness of the stellar cusp, as more stars are available near the disk to torque

it. For example, $P_8 = 0.02, 0.11$ and 0.29 for $i_0 = 0$ rad $\chi = 1$ in a sequence of models with $\gamma = 3/2, 7/4$ and 2 , respectively.

We find that for the $i_0 = 0$ rad models of NGC 4258, the rms RR-induced misalignment between the MBH spin axis and the disk's total angular momentum is $\text{rms}(i) = 15^\circ$ after 10^8 yr for the case $\chi = 1$, and as large as $\text{rms}(i) = 44^\circ$ for the $\chi = 0$ case. This is an example of the stabilizing effect of the BP torques, which introduce a preferred plane for the disk, and suppress warps. It is interesting to note that the observed maser disk in NGC 4258 is tilted by $\sim 30^\circ$ to the present jet axis, as identified by the North and South hotspots (Cecil et al. 2000; Wilson et al. 2001). Assuming that the jet is aligned with the MBH spin axis, then such a tilt is consistent with RR torquing of a disk (see Figure 1d), possibly around a sub-maximal spinning MBH.

The warping of the disk exposes it to ionizing radiation from its innermost parts, which may play a central role in determining the physical conditions in the outer regions of the disk. The fraction of the central luminosity that falls on the disk (assuming isotropic emission) is expressed by the disk's covering fraction, $C_f = \int_0^{2\pi} d\phi |\cos \theta_{\text{max}}(\phi) - \cos \theta_{\text{min}}(\phi)| / 4\pi$, where θ_{min} and θ_{max} are the minimal and maximal inclinations above and below the disk's mean plane along R in azimuthal direction ϕ . Figure (3) shows that RR-induced warping gives the disk a minimal varying covering factor of $C_f \sim 0.1 - 0.3$, on top of any contribution from a pre-existing large scale warp (e.g by the BP effect).

3.2. Mass accretion rate

As noted by Lodato & Pringle (2006), warping increases the mass accretion rate over that in a flat disk because of the additional dissipation due to the vertical shear. We confirm here that the warps are associated with mass accretion fluctuations of up to factors of 3–4 over that in a flat disk (Figure 2), resulting in an overall increase by a factor of up to $f_{\dot{M}} \sim 1.4$ in the average mass accretion rate. The power spectrum of the accretion rate fluctuations in the maser model is very broad (Figure 4), and can be roughly approximated by a broken power-law, which flattens beyond $\gtrsim 10^7$ yr. This timescale corresponds to the RR coherence time in the outer half of the disk, $r \lesssim R_d = 0.16$ pc to $r \sim R_2 = 0.27$ pc. A rough estimate of this variability timescale can be obtained by evaluating the coherence time at the disk's mass-weighted mean radius, since that is where the gravitational coupling with the stars is maximal. That length-scale is typically in the regime where the back-reaction time is shorter than the self-quenching time (Eq.9), and so

$$t_{\text{var}} \sim t_{\text{react}}(R_d) \sim (M_\bullet/M_d)P(R_d) \simeq 1.1 \times 10^7. \quad (21)$$

A similar correspondence is seen between the variability timescale of the AGN model (Section 3.3), $t_{\text{var}} \simeq 1240$, and the power-law break in its power spectrum (Figure 4). Thus, t_{var} can be interpreted as the shortest timescale for which there is substantial variability power.

3.3. MBH spin evolution

The enhanced mass accretion rate translates directly to a faster rate of change in the magnitude of the the MBH spin, $\dot{J}_\bullet \simeq \dot{M}\sqrt{GM_\bullet/R_d}$, as the MBH spin vector remains aligned with the inner regions of the disk due to the BP torques. The BP torques also couple the fluctuating RR torques on the disk to the MBH spin orientation (Figure 5, 15). For the effect

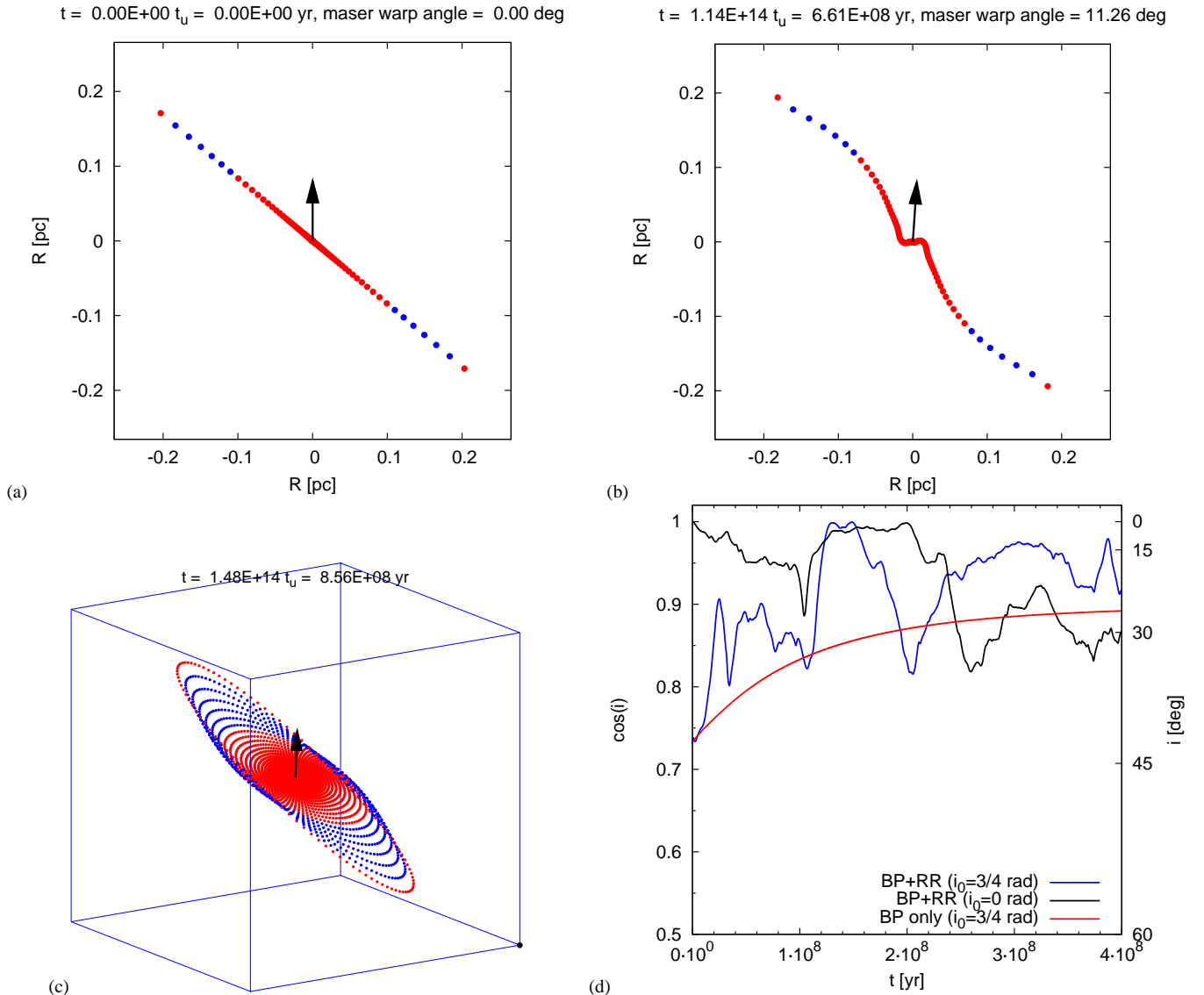


FIG. 1.— Top row and bottom left: Snapshots from a disk evolution simulation of NGC 4258 with $\alpha_1 = 0.25$, $\chi = 1$, Kramer’s opacity law, and the initial conditions $\mathbf{J}_\bullet = \hat{z}$ and $i_0 = 3/4$ rad. The arrow denotes the MBH spin vector. The maser region is marked in blue. Top: The intersection of the disk mid plane with the $x - z$ plane (the simulated plane of sky). Bottom left: The disk mid plane in 3D. Bottom right: The evolution of $\cos i$ in the simulation shown in the snapshots, and for similar simulations with $i_0 = 0$ rad, and with BP torques only ($N_\star = 0$).

to be significant, the disk must be massive enough to carry a substantial amount of angular momentum (Eqs. 14, 15), but not so massive as to remain effectively immobile against the RR torques.

We find that the response of the MBH spin in NGC 4258 to the BP torques is very small, because of the very low mass of the disk. However, the effect can be larger in systems with a more massive accretion disk. Figure (5) shows as an example the evolution of the MBH spin axis relative to its initial direction (we omit the much smaller spin evolution due to accretion), and that of the total angular momentum of the disk, for a low-mass luminous AGN model that corresponds to a Seyfert galaxy ($L \sim 7 \times 10^{43}$ ergs $^{-1}$ for a radiative efficiency of $\eta = 0.1$). The angular momenta of the MBH and the disk both execute a random walk around their initial orientation. The amplitude of the disk angular momentum jitter is larger than that of the MBH spin, because the RR coherence time, $t_{\text{react}} = 620$ yr at $R_d = 2.2 \times 10^{-3}$ pc is much shorter than the BP timescale $t_{\parallel} = 4.1 \times 10^5$ yr, and so the MBH spin cannot

“catch up” with the faster changes in the direction of the stellar torques. We find that for this specific model, the MBH spin scatters across $\sim 5^\circ$ over an e -folding time (4.5×10^7 years). Another consequence of the short coherence time (compared to $t_{\text{warp}}(R_d) \simeq 3.5 \times 10^4$ yr) is that the RR-induced warps in this disk model have angles of only $\sim 1^\circ$. Their effect on the mass accretion rate is correspondingly small, only a $\sim 2\%$ increase over that in a flat disk.

4. DISCUSSION AND SUMMARY

4.1. Discussion

A circumnuclear accretion disk does not exist in isolation around a MBH. Rather, it shares the volume with the high-density nuclear cluster that is predicted to form there while the nucleus evolves. The cluster is expected to be on average spatially isotropic near the MBH, but the Poisson fluctuations in the distribution of orbital inclinations lead to a slowly varying residual force that exerts coherent torques on the disk (RR). We argue (Section 1.3) that a thin Keplerian disk is primar-

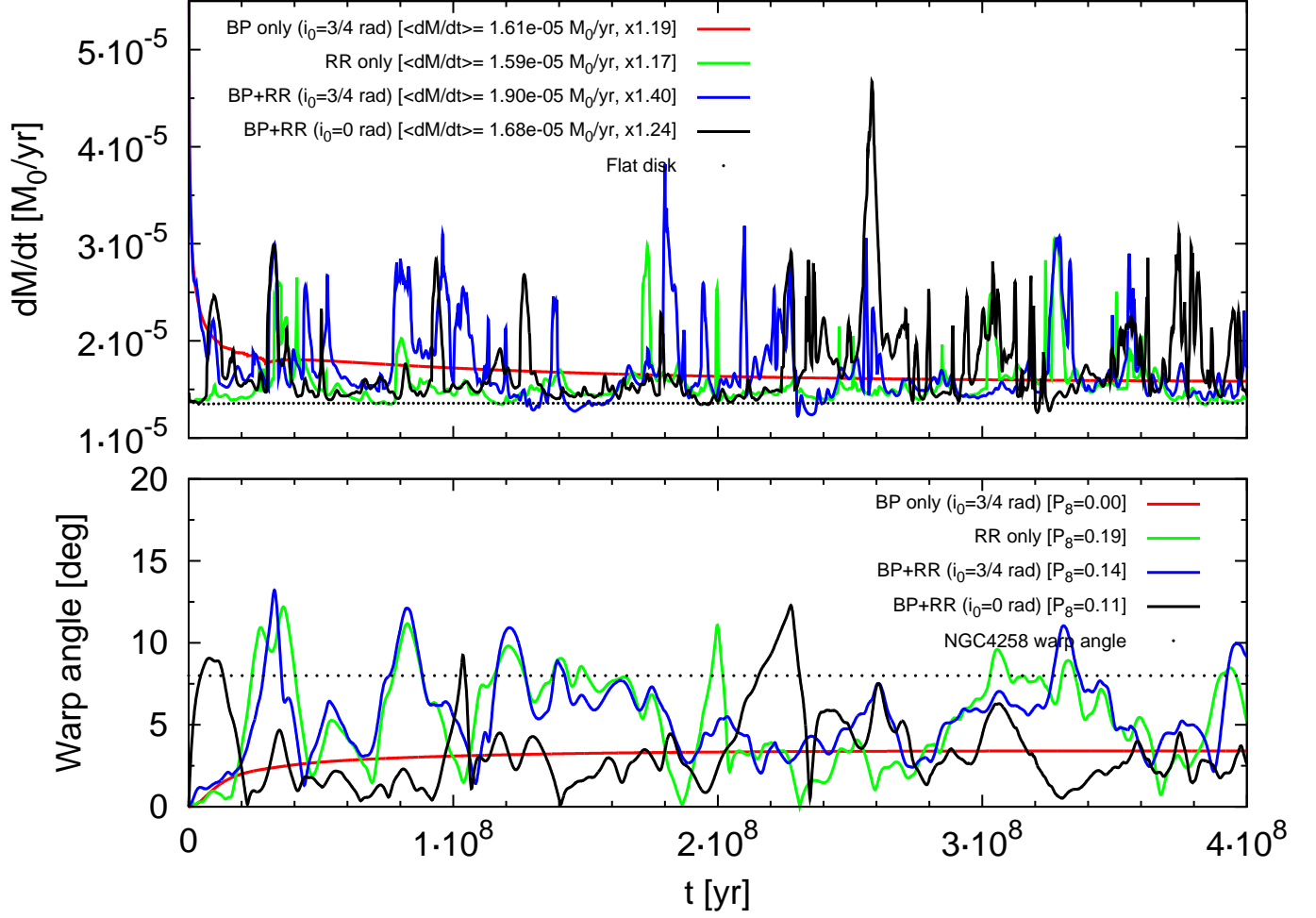


FIG. 2.— Simulated disk evolution with $\alpha_1 = 0.25$, $\chi = 0$ or 1 and with Kramer’s opacity law, for the cases of BP warping only ($N_* = 0$), RR warping only ($\chi = 0$) and both BP and RR warping (all models have the same RR realization and initial MBH spin $\mathbf{J}_\bullet = \hat{z}$ and $i_0 = 0$ or $3/4$ rad. They were evolved over 10^9 yr, of which the initial 4×10^8 yr are shown). Top: The mass accretion rate. The mass loss rate from the equivalent steady state flat disk, $\dot{M} = 1.4 \times 10^{-5} M_\odot \text{yr}^{-1}$, is also shown for reference. The mean mass loss rates, and their enhancement over that of a steady state flat disk are indicated in the plot labels. Bottom: The warp angle across the maser zone. The best fit warp angle of $\omega = 8^\circ$ for NGC 4258 (Herrnstein et al. 2005) is shown for reference. The fraction of time the models spend with a warp as large as that observed, P_8 , are indicated in the plot labels.

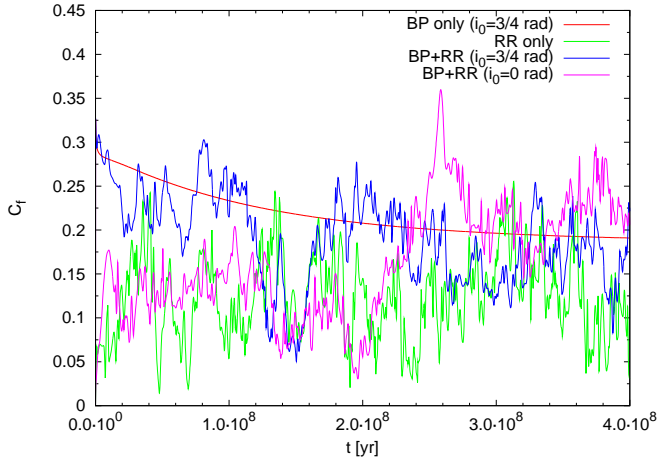


FIG. 3.— The evolution of the maser disk’s covering factor due to BP and RR for the models shown in Figure (2).

ily torqued by these purely gravitational interactions with the stars, rather than by the hydrodynamical ones that occur when stars plunge through the disk. The RR torques warp the disk and can lead to order unity variability in the disk geometry

(Figs. 1, 2), its mass accretion rate (Figs. 2, 4) and covering factor (Figure 3). The strong coupling between the stellar potential fluctuations and the disk via RR is then further extended to the MBH spin via the frame-dragging BP effect, and this allows angular momentum to be transferred from the nuclear cluster to the MBH. The combined effects of the perpendicular RR and BP torques excite a jitter in the MBH spin direction (Figure 5). In addition, the increased mass accretion rate due to the RR-induced warping, together with the disk / MBH spin alignment due to the BP effect, lead to an increased growth rate of the MBH spin magnitude. We conclude that gravitational interactions between the stars and the disk excite a substantial level of irreducible variability in the disk properties—stationary accretion in a circumnuclear disk is merely an idealization.

The large-scale warping of the disk (for NGC 4258, this coincides with the maser region warp) reflects the RR coherence timescale at the mass-weighted mean disk radius, $t_{\text{var}} \sim (M_\bullet/M_d)P(R_d)$ yr ($\sim 10^7$ yr for NGC 4258). Generally, the effect of RR on the disk and the MBH will be substantial when the disk is long-lived, $t_{\text{disk}} > t_{\text{var}}$. There is a large spread in the estimates of AGN and QSO lifespans in the

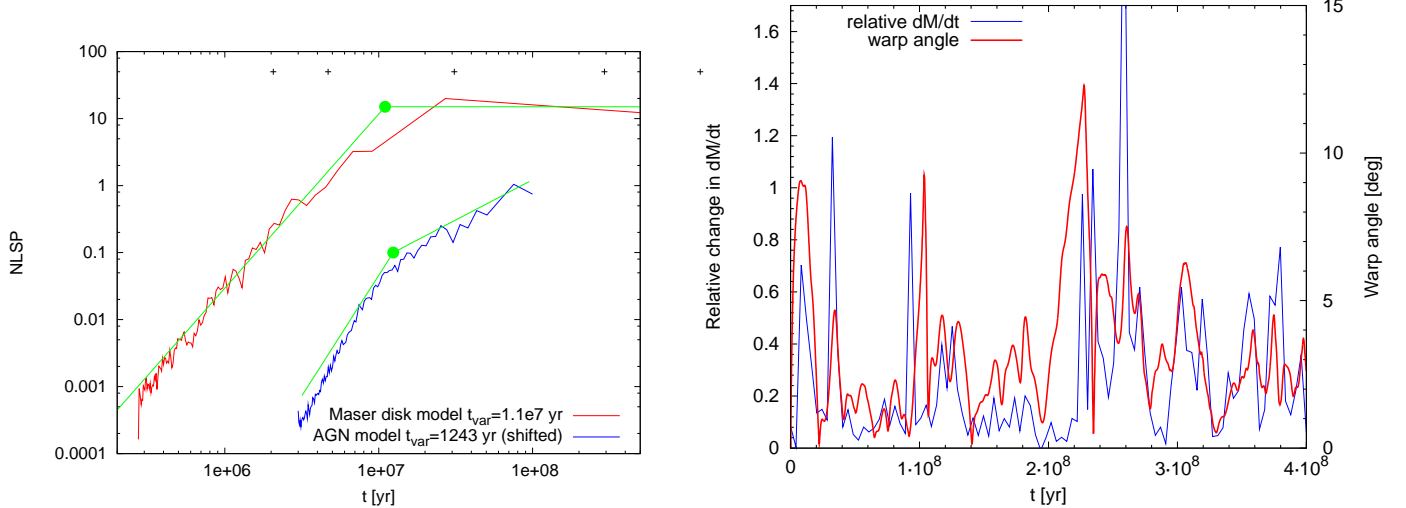


FIG. 4.— Left: The smoothed Normalized Lomb-Scargle Periodograms (power spectra) of $\dot{M}(t)$, as function of inverse frequency, for the NGC 4258 maser disk model and for the AGN model discussed in Section 3.3. The coherence times of the star shells that are used to simulate the RR torques (Section 2.3.2) for the maser disk model are marked by crosses. The periodograms were smoothed to highlight the power-law break at t_{var} (green line and circle), which indicates that most of the power is at $t \gtrsim t_{\text{var}} = (M_{\bullet}/M_d)P(R_d)$ (The AGN model is displayed shifted on the logarithmic scale for comparison with the maser disk model). Right: The correlation between the variability on the large (maser region) scale and the relative mass accretion rate (normalized to the steady state case) in a model of NGC 4258 (BP and RR, $i_0 = 0$ rad and $\chi = 1$). The mass accretion rate curve was smoothed by cubic spline, to filter out the short time-scale variability (cf Figure 2) and highlight the correlation between warping and mass accretion rate on longer time scales.

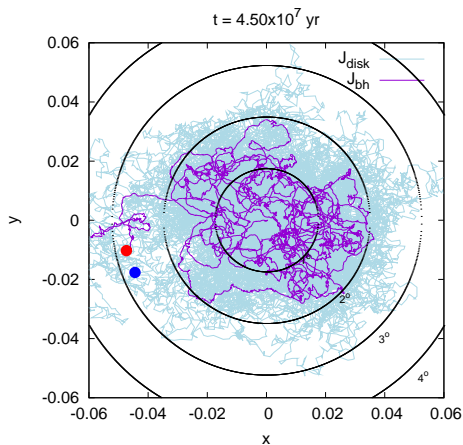


FIG. 5.— The evolution of the MBH spin \mathbf{J}_{\bullet} , and the disk's total angular momentum \mathbf{J}_{disk} , over an e -folding time (for $\eta = 0.1$), shown projected on the (x, y) plane, under the influence of BP and RR together, for a low mass AGN model with $M_{\bullet} = 4 \times 10^6 M_{\odot}$, $r_h = 2.3$ pc, $\mu_h = 2$, $\gamma = 2$, $\alpha_1 = 0.1$, $\chi = 1$, Kramer's opacity law, normalized with $[H/R]_a = 0.002$, $\rho_a = 2.4 \times 10^{-12}$, $T_a = 1000$ K and $\kappa_a = 10 \text{ cm}^2 \text{ g}^{-1}$ at $R_a = 0.1$ pc, and the initial conditions $\mathbf{J}_{\bullet} = \hat{z}$ and $i = 0$ rad. These parameters result in $M_d = 1.6 \times 10^4 M_{\odot}$, $R_d = 2.2 \times 10^{-3}$ pc, $t_{\text{var}} \simeq 1240$ yr, $\dot{M} = 0.013 M_{\odot} \text{ yr}^{-1} = 1.4 \eta \dot{M}_E$, $R_{\text{BP}} = 3.6 \times 10^{-4}$ pc, and $t_{\parallel} = 4.1 \times 10^5$ yr. The blue and red circles denote the projection of \mathbf{J}_{\bullet} and \mathbf{J}_{disk} , respectively, at the end of the simulation.

luminous phase, $\text{few} \times 10^6 - 10^8$ yr (e.g. Grazian et al. 2004; Porciani et al. 2004), with some recent analyses suggesting an even longer lifespan of $\lesssim 10^9$ yr (Gilli et al. 2009; Ross et al. 2009; Schawinski et al. 2009). For long-lived disk systems, the cumulative effects of RR-torquing can be large.

One implication of the factor $f_{\dot{M}} \sim 1.2 - 1.4$ increase in the mean mass accretion rate over that in a flat stationary disk (Section 3.2), is that an MBH fed by an RR-torqued disk, whose mass accretion rate is raised to the Eddington limit by warping, will be $\exp[(f_{\dot{M}} - 1)(t_{\text{disk}}/t_E)]$ more massive than one that is fed by an otherwise identical flat disk, which is accreting at only $1/f_{\dot{M}}$ of the Eddington limit. For exam-

ple, RR-torquing can accelerate MBH growth over a time $t_{\text{disk}} = 10t_E = 4.5 \times 10^8$ yr (assuming $\eta = 0.1$) by a factor of up to ~ 50 (for $f_{\dot{M}} = 1.4$). Alternatively, if radiation pressure prevents the increased RR-induced mass flow from accreting on the MBH, the accumulating excess mass may trigger outflows, or disk fragmentation and star formation.

Another cumulative effect of RR-torquing of the disk is the displacement of the MBH spin from its initial orientation due to the BP-induced random jitter. It is interesting to note that the few degrees amplitude of the displacement is still consistent with the typical observed $\sim 5^\circ$ opening angle of AGN radio jets on large scales (Oppenheimer & Biretta 1994), assuming the jet direction reflects the spin direction.

A direct geometric consequence of RR-induced warping is the substantial time-averaged covering factor the disk acquires relative to the central continuum source. This allows the disk to intercept the central radiation and be heated and ionized by it. Such X-ray irradiation may in fact be essential for raising the gas temperature to the range necessary for maser emission (Neufeld & Maloney 1995), for the production of the observed emission lines in AGN disks in general (Collin-Souffrin 1987), for driving winds and outflows from disks (Proga & Kallman 2004), or for explaining Narrow Line Seyfert 1 galaxies and ultra-soft AGN (Puchnarewicz & Soria 2002).

The magnitude of the effects of the stars on the disk depend on the central concentration of the stellar cluster, and is therefore sensitive to the degree of mass segregation in the system and to the fraction of massive compact remnants in the population. The more centrally concentrated the stellar density profile, and the more massive the stars (for RR, the relevant quantity is $\langle M_{\star}^2 \rangle / \langle M_{\star} \rangle$, Rauch & Tremaine 1996), the larger are the effects on the disk. It is worth noting that strong mass segregation with a power-law cusp profiles of $\gamma \gtrsim 2$ is expected to occur in nuclei with old stellar populations (Alexander & Hopman 2009; Keshet et al. 2009; Preto & Amaro-Seoane 2010), where the inner parts of the cusp are dominated by stellar black holes of mass $O(10 M_{\odot})$.

It is thus plausible that a substantial fraction of galactic nuclei have conditions that are conducive to RR-torquing of an accretion disk.

In this study we presented numerical results for galactic nuclei with MBH masses in the range $\sim 4 \times 10^6 M_\odot$ (with a massive disk close to \dot{M}_E) to $\sim 4 \times 10^7 M_\odot$ (with a low-mass, low-accretion rate disk). In order to scale the results to other systems, it is necessary to specify the scaling of the disk properties with MBH mass. We defer this to future work, and present here only a simple preliminary analysis that suggests that the effects are generally more important in lower-mass MBHs. Assuming that all AGN disks extend up to some universal large multiple of r_g (e.g. $\sim 2000 r_g$ for α -disks limited by gravitational instability, Goodman 2003), and assuming they all have the same aspect ratio, then $R_d \propto M_\bullet$ and $M_d/M_\bullet \simeq H/R$, so that $M_d \propto M_\bullet$. The angular momentum in the disk therefore scales as $J_d \propto M_d \sqrt{M_\bullet R_d} \propto M_\bullet^2$. The M_\bullet/σ relation indicates that the MBH radius of influence scales as $r_h \propto M_\bullet^{1/2}$ (assuming $M_\bullet \propto \sigma^4$), so that the number of stars in the MBH cusp inside R_d scales as $N_*(R_d) \propto M_\bullet (R_d/r_h)^{3-\gamma} \propto M_\bullet^{(5-\gamma)/2}$. The residual angular momentum in the stars that are efficiently coupled to the disk then scales as $J_N \propto \sqrt{N_*(R_d)} \sqrt{M_\bullet R_d} \propto M_\bullet^{(9-\gamma)/4}$, and it then follows that $J_d/J_N \propto M_\bullet^{(\gamma-1)/4}$. The ratio of the disk and stellar angular momenta is a slowly rising function of M_\bullet for $\gamma > 1$. This implies that, all other parameters being equal, it should become progressively more difficult for the stars to torque the disk as the MBH mass increases. In addition, as argued in Section (1.3), the larger M_\bullet , the more the disk responds to the RR torques as a rigid body, rather than by growing warps.

4.2. Caveats

The calculations and conclusions presented here are limited by various assumptions and approximations. They are listed here briefly. Some of these issues will be addressed in future work.

Limitations of the galactic nucleus model— The RR torques by the stellar cluster are approximated by the gravitational field of a small number of thin rings (Section 2.3.2), which provides only a rough approximation of the true power spectrum of the stellar perturbations. The back-reaction of the disk on the stars is approximated simplistically by limiting the RR coherence time so it does not exceed the back-reaction time. A more realistic fluctuation spectrum will allow, among other issues, to better model the very short timescale fluctuations, and explore whether these have any relation to the observed optical/UV variability of AGN. Our conclusions on mass accretion rates and MBH spin evolution are generalizations based on extrapolating simulations that were constructed explicitly to represent the disk and cluster of NGC 4258. They should be scaled and tested for a wider range of MBHs, disks and nuclear clusters.

Limitations of the disk model— The physics underlying accretion disks are still not well understood. In particular

the nature of the azimuthal and vertical viscosities, and the relation between them, are quite uncertain (Ogilvie 1999; Lodato & Pringle 2007; Lodato & Price 2010). The disk is not modeled self-consistently. The thermal structure of the disk is based for simplicity on a Kramer opacity law with a free normalization constant, which is clearly non-physical, as indicated by the very high opacity that is required to produce the masing conditions. External X-ray heating, which is likely important, is neglected. MBH spin evolution due to mass accretion can be relevant on longer timescales, but is not taken into account, and the artificial BP torque suppression on small scales that is needed to stabilize the results numerically, may both lead to an underestimation of the effect of disk warping on the MBH spin evolution. Finally, the disk is approximated as Newtonian and Keplerian, even near the ISCO, which is held fixed at its Schwarzschild value.

Limitations of the numerical scheme— The numerical scheme used here (Papaloizou & Pringle 1983; Pringle 1992) can not describe azimuthal modes and as implemented, is limited to moderate warp angles (although viscosities for arbitrary large angles can be calculated numerically, Ogilvie 1999). In particular, disk flipping from co-rotation to counter-rotation, or disk destruction by large deformations, cannot be modeled reliably.

4.3. Summary

We analyzed and simulated numerically the evolution of a thin accretion disk around a MBH that is surrounded by a stellar cluster. We took into account the disk's internal viscous torques, the frame-dragging torques of a spinning MBH and the stellar orbit-averaged gravitational torques. We show that the evolution of the MBH mass accretion rate, the MBH spin growth rate, and the covering fraction of the disk relative to the central ionizing continuum source, are all strongly coupled to the stochastic fluctuations of the stellar potential via the warps that the stellar torques excite in the disk. These lead to fluctuations by factors of up to a few in these quantities over a wide range of timescales, with most of the power on timescales $\gtrsim (M_\bullet/M_d)P(R_d)$. The response of the disk is stronger the lighter it is and the more centrally concentrated the stellar cusp. We demonstrated these effects by simulating the evolution of the maser disk in NGC 4258, and show that its observed $O(10^\circ)$ warp can be driven by the stellar torques. We also show that the frame-dragging of a massive AGN disk couples the stochastic stellar torques to the MBH spin and can excite a jitter of a few degrees in its direction relative to that of the disk's outer regions.

We thank J. Cuadra, J. Granot, K. Gültekin J.-P. Lasota, A. Levinson, G. Lodato, C. Nixon and F. Pedes for helpful discussions and comments. T.A. acknowledges support by ERC Starting Grant 202996 and DIP-BMBF grant 71-0460-0101.

APPENDIX

A. THE DISCRETIZED DISK EVOLUTION EQUATION

The integration of the evolution equation generally follows the scheme of Pringle (1992), but some details of the implementation are different. It is presented here briefly for completeness.

All quantities are expressed in a system of units where $G = c = M_\bullet = 1$. Denoting by Δz the equal spacing of the logarithmic

grid, the grid points are at $R_i = R_1 e^{(i-1)\Delta z}$ for $i = 0, \dots, N+1$, where points R_0, R_{N+1} represent the boundaries and $R_1 = 6$ is at the ISCO. The angular momenta densities at time t_j , \mathbf{L}_i^j ($i = 1, \dots, N$), are advanced in time to $t_{j+1} = t_j + \Delta t_j$ by

$$\begin{aligned} \mathbf{L}_i^{j+1} = & \mathbf{L}_i^j + \frac{\Delta t_j}{(\Delta z)^2 R_i^2} \\ & \times \left\{ 3 \left[\left(v_{1,i+1}^j \mathbf{L}_{i+1}^j - v_{1,i}^j \mathbf{L}_i^j \right) \bar{\boldsymbol{\ell}}_{i,i+1}^j - \left(v_{1,i}^j \mathbf{L}_{i-1}^j - v_{1,i-1}^j \mathbf{L}_{i-1}^j \right) \bar{\boldsymbol{\ell}}_{i-1,i}^j \right] \right. \\ & + \frac{1}{2} \left[\bar{v}_{2,i,i+1}^j \bar{\mathbf{L}}_{i,i+1}^j (\boldsymbol{\ell}_{i+1}^j - \boldsymbol{\ell}_i^j) - \bar{v}_{2,i-1,i}^j \bar{\mathbf{L}}_{i-1,i}^j (\boldsymbol{\ell}_i^j - \boldsymbol{\ell}_{i-1}^j) \right] \\ & - \Delta z \left[V_{\text{adv},k+1}^j R_{k+1} \mathbf{L}_{k+1}^j - V_{\text{adv},k}^j R_k \mathbf{L}_k^j \right] \\ & \left. + \left[\bar{v}_{3,i,i+1}^j \bar{\mathbf{L}}_{i,i+1}^j \times (\boldsymbol{\ell}_{i+1}^j - \boldsymbol{\ell}_i^j) - \bar{v}_{3,i-1,i}^j \bar{\mathbf{L}}_{i-1,i}^j \times (\boldsymbol{\ell}_i^j - \boldsymbol{\ell}_{i-1}^j) \right] \right\} \end{aligned} \quad (\text{A1})$$

$$+ \Delta t_j \mathbf{T}_{\text{ext},i}^j, \quad (\text{A2})$$

where $\bar{\mathbf{L}}_{i,i+1}^j = (\mathbf{L}_i^j + \mathbf{L}_{i+1}^j)/2$, $\bar{\boldsymbol{\ell}}_{i,i+1}^j = \bar{\mathbf{L}}_{i,i+1}^j / |\bar{\mathbf{L}}_{i,i+1}^j|$, and $\bar{v}_{n,i,i+1}^j = (v_{n,i}^j + v_{n,i+1}^j)/2$ for $n = 2, 3$. The index k is defined as $k = i - 1$ when the advective velocity $V_{\text{adv},i}^j > 0$, and $k = i$ when $V_{\text{adv},i}^j < 0$, where

$$V_{\text{adv},i}^j = \frac{1}{R_i} \left[\frac{3}{2} v_{1,i} - v_{2,i} \left| \frac{\boldsymbol{\ell}_{i+1} - \boldsymbol{\ell}_{i-1}}{2\Delta z} \right|^2 \right], \quad (\text{A3})$$

for $i = 1, \dots, N$. For $i = 0, i - 1$ in Eq. (A3) is substituted by 0, and for $i = N + 1, i + 1$ is substituted by $N + 1$. The viscosities (and all other thermodynamic properties) are then updated via Eq. (17).

The inner boundary conditions, $\mathbf{L}(R_1) = 0$, $\partial \boldsymbol{\ell} / \partial R|_{R_1} = 0$ are enforced by setting $\mathbf{L}_0^j = 0$ (this causes a slight deviation from the analytic solution, since $\mathbf{L}_1^j \rightarrow 0$, but is not zero identically), and $\boldsymbol{\ell}_0^j = \boldsymbol{\ell}_1^j$. The outer boundary condition, $\partial(v_1 \mathbf{L}) / \partial R = 0$ is enforced by setting $\mathbf{L}_{N+1}^j = (v_{1,N}^j / v_{1,N+1}^j) \mathbf{L}_N^j$. The mass-loss from the inner edge of the disk is balanced (in the statistical sense) by adding a source term at the outer radius, $\mathbf{L}_N^j \rightarrow \mathbf{L}_N^j + (\Delta L_N)^j \boldsymbol{\ell}_0$ (see Section 2.3.1 and Eq. 18).

The time-step size is adjusted every time-step to

$$\Delta t_j = \min(\Delta t_{v_1}^j, \Delta t_{v_2}^j, \Delta t_{v_3}^j, \Delta t_{\text{BP}}^j, \Delta t_{\text{RR}}^j) / 2, \quad (\text{A4})$$

where

$$\begin{aligned} \Delta t_{v_n}^j &= \min_i (\Delta R_i)^2 / \bar{v}_{n,i,i+1}^j \quad \text{for } n = 1, 2, 3, \\ \Delta t_{\text{BP}}^j &= \min_i L_i^j / |\mathbf{T}_{\text{BP},i}^j|, \quad \Delta t_{\text{RR}}^j = \min_i (M_\star / M_\bullet) / \sqrt{N_\star (< R_i) R_i^3 / 2}, \end{aligned} \quad (\text{A5})$$

and where $\bar{v}_{1,i,i+1}$ is defined similarly to $\bar{v}_{2,i,i+1}$.

Angular momentum conservation is monitored by evaluating the change in the total angular momentum of the disk between times t_{j-1} and t_j in two different ways. One, which corresponds to the divergence term in the continuity equation, is $\Delta \mathbf{J}_{\text{edge}}^j (\mathbf{L}_0^j, \mathbf{L}_1^j, \mathbf{L}_N^j, \mathbf{L}_{N+1}^j, \mathbf{L}_0^{j-1}, \mathbf{L}_1^{j-1}, \mathbf{L}_N^{j-1}, \mathbf{L}_{N+1}^{j-1}) = -2\pi \sum_{i=0}^{N+1} R_i \Delta R_i (\mathbf{L}_i^j - \mathbf{L}_i^{j-1})$, which can be written as a function of the disk edges only, since all the inner grid points cancel out in the sum. The other, which corresponds to the time derivative term in the continuity equation, is the change of angular momentum in the bulk, $\Delta \mathbf{J}_{\text{bulk}}^j = \mathbf{J}_{\text{bulk}}^j - \mathbf{J}_{\text{bulk}}^{j-1}$, where $\mathbf{J}_{\text{bulk}}^j = 2\pi \sum_{i=1}^N R_i \Delta R_i \mathbf{L}_i^j$. The fractional degree of non-conservation per time-step in the absence of source terms (Section 2.3.3) is then $\delta J^j = \left| \Delta \mathbf{J}_{\text{bulk}}^j + \Delta \mathbf{J}_{\text{edge}}^j \right| / J_{\text{bulk}}^{j-1}$. Analogous expressions are used to monitor mass conservation.

B. SECOND ORDER COEFFICIENTS OF THE VISCOSITY PARAMETER EXPANSION

The expansion of the dimensionless viscosity parameters (Eq. 12) was derived by Ogilvie (1999). The second order coefficients are reproduced here for convenience in the notation of this paper, as functions of the in-plane shear viscosity parameter α_1 and the adiabatic index Γ only ($\Gamma = 7/5$ for diatomic gas). The dependence on a bulk viscosity parameter, assumed here to be zero, is not included.

$$B_1 = \frac{-2(1 - 17\alpha_1^2 + 21\alpha_1^4)}{12\alpha_1(4 + \alpha_1^2)}, \quad B_2 = 2\text{Re}(Q_{23}), \quad B_3 = \text{Im}(Q_{23}), \quad (\text{B1})$$

where

$$Q_{23} = \frac{\tilde{a} + \tilde{b}\Gamma + \tilde{c}[\Gamma - (8/3)\alpha_1 i]}{4\alpha_1[3 - \Gamma + (8/3)\alpha_1 i](-\alpha_1 + 2i)^3(\alpha_1 + 2i)}, \quad (\text{B2})$$

and

$$\begin{aligned} \tilde{a} &= (12 + 49\alpha_1^2 - 408\alpha_1^4 + 2\alpha_1^6) + (115 + 109\alpha_1^2 - 41\alpha_1^4 + 4\alpha_1^6)\alpha_1 i, \\ \tilde{b} &= (18 - 87\alpha_1^2 - 24\alpha_1^4) + (87 - 6\alpha_1^4)\alpha_1 i, \\ \tilde{c} &= (12 - 36\alpha_1^2 + 140\alpha_1^4 + 2\alpha_1^6) + (25 - 11\alpha_1^2 + 21\alpha_1^4)\alpha_1 i. \end{aligned} \quad (\text{B3})$$

REFERENCES

- Alexander, T. & Hopman, C. 2009, *ApJ*, 697, 1861
 Argon, A. L., Greenhill, L. J., Reid, M. J., Moran, J. M., & Humphreys, E. M. L. 2007, *ApJ*, 659, 1040
 Arnett, D. 1996, *Supernovae and Nucleosynthesis: An Investigation of the History of Matter from the Big Bang to the Present*, ed. Arnett, D. (Princeton University Press: Princeton, NJ)
 Artymowicz, P., Lin, D. N. C., & Wampller, E. J. 1993, *ApJ*, 409, 592
 Bahcall, J. N. & Wolf, R. A. 1976, *ApJ*, 209, 214
 —. 1977, *ApJ*, 216, 883
 Bardeen, J. M. & Petterson, J. A. 1975, *ApJ*, 195, L65+
 Braatz, J. A. & Gugliucci, N. E. 2008, *ApJ*, 678, 96
 Bregman, M. & Alexander, T. 2009, *ApJ*, 700, L192
 Caproni, A., Abraham, Z., Livio, M., & Mosquera Cuesta, H. J. 2007, *MNRAS*, 379, 135
 Cecil, G., Greenhill, L. J., DePree, C. G., Nagar, N., Wilson, A. S., Dopita, M. A., Pérez-Fournon, I., Argon, A. L., & Moran, J. M. 2000, *ApJ*, 536, 675
 Collin-Souffrin, S. 1987, *A&A*, 179, 60
 Eilon, E., Kupi, G., & Alexander, T. 2009, *ApJ*, 698, 641
 Ferrarese, L. & Merritt, D. 2000, *ApJ*, 539, L9
 Frank, J., King, A., & Raine, D. J. 2002, *Accretion Power in Astrophysics*, third edn. (Cambridge University Press)
 Gebhardt, K. et al. 2003, *ApJ*, 583, 92
 Gilli, R. et al. 2009, *A&A*, 494, 33
 Goodman, J. 2003, *MNRAS*, 339, 937
 Grazian, A., Negrello, M., Moscardini, L., Cristiani, S., Haehnelt, M. G., Matarrese, S., Omizzolo, A., & Vanzella, E. 2004, *AJ*, 127, 592
 Greenhill, L. J., Jiang, D. R., Moran, J. M., Reid, M. J., Lo, K. Y., & Claussen, M. J. 1995, *ApJ*, 440, 619
 Greenhill, L. J. et al. 2003, *ApJ*, 590, 162
 Gürkan, M. A. & Hopman, C. 2007, *MNRAS*, 379, 1083
 Herrnstein, J. R., Greenhill, L. J., & Moran, J. M. 1996, *ApJ*, 468, L17+
 Herrnstein, J. R., Moran, J. M., Greenhill, L. J., & Trotter, A. S. 2005, *ApJ*, 629, 719
 Herrnstein, J. R. et al. 1999, *Nature*, 400, 539
 Hopman, C. & Alexander, T. 2006, *ApJ*, 645, 1152
 Keshet, U., Hopman, C., & Alexander, T. 2009, *ApJ*, 698, L64
 King, A. R., Lubow, S. H., Ogilvie, G. I., & Pringle, J. E. 2005, *MNRAS*, 363, 49
 Kocsis, B. & Tremaine, S. 2011, *MNRAS*, 412, 187
 Kondratko, P. T., Greenhill, L. J., & Moran, J. M. 2008, *ApJ*, 678, 87
 Lo, K. Y. 2005, *ARA&A*, 43, 625
 Lodato, G. & Price, D. J. 2010, *MNRAS*, 405, 1212
 Lodato, G. & Pringle, J. E. 2006, *MNRAS*, 368, 1196
 —. 2007, *MNRAS*, 381, 1287
 Maloney, P. R. 2002, *Pub. Astron. Soc. Australia*, 19, 401
 Martin, R. G. 2008, *MNRAS*, 387, 830
 Merritt, D. 2006, *Reports on Progress in Physics*, 69, 2513
 Nayakshin, S. 2005, *MNRAS*, 359, 545
 Neufeld, D. A. & Maloney, P. R. 1995, *ApJ*, 447, L17+
 Ogilvie, G. I. 1999, *MNRAS*, 304, 557
 Oppenheimer, B. R. & Biretta, J. A. 1994, *AJ*, 107, 892
 Papaloizou, J. C. B. & Pringle, J. E. 1983, *MNRAS*, 202, 1181
 Porciani, C., Magliocchetti, M., & Norberg, P. 2004, *MNRAS*, 355, 1010
 Preto, M. & Amaro-Seoane, P. 2010, *ApJ*, 708, L42
 Pringle, J. E. 1992, *MNRAS*, 258, 811
 Proga, D. & Kallman, T. R. 2004, *ApJ*, 616, 688
 Puchnarewicz, E. M. & Soria, R. 2002, *arXiv:astro-ph/0202030*
 Rauch, K. P. & Ingalls, B. 1998, *MNRAS*, 299, 1231
 Rauch, K. P. & Tremaine, S. 1996, *New Astronomy*, 1, 149
 Ross, N. P., Shen, Y., Strauss, M. A., Vanden Berk, D. E., Connolly, A. J., Richards, G. T., Schneider, D. P., Weinberg, D. H., Hall, P. B., Bahcall, N. A., & Brunner, R. J. 2009, *ApJ*, 697, 1634
 Schawinski, K., Virani, S., Simmons, B., Urry, C. M., Treister, E., Kaviraj, S., & Kushkuley, B. 2009, *ApJ*, 692, L19
 Semenov, D., Henning, T., Helling, C., Ilgner, M., & Sedlmayr, E. 2003, *A&A*, 410, 611
 Shakura, N. I. & Sunyaev, R. A. 1973, *A&A*, 24, 337
 Shields, G. A., Gebhardt, K., Salviander, S., Wills, B. J., Xie, B., Brotherton, M. S., Yuan, J., & Dietrich, M. 2003, *ApJ*, 583, 124
 Shirley, Y. L., Huard, T. L., Pontoppidan, K. M., Wilner, D. J., Stutz, A. M., Biegging, J. H., & Evans, II, N. J. 2011, *ApJ*, 728, 143
 Soltan, A. 1982, *MNRAS*, 200, 115
 Syer, D., Clarke, C. J., & Rees, M. J. 1991, *MNRAS*, 250, 505
 Toomre, A. 1964, *ApJ*, 139, 1217
 Vilkoviskij, E. Y. & Czerny, B. 2002, *A&A*, 387, 804
 Wilson, A. S., Yang, Y., & Cecil, G. 2001, *ApJ*, 560, 689
 Young, P. 1980, *ApJ*, 242, 1232
 Yu, Q. & Tremaine, S. 2002, *MNRAS*, 335, 965

